YIPFα1A expression is regulated by multilayered molecular mechanisms

Tokio Takaji[1,2], Yurika Nakanishi[1], Nobuhiro Nakamura[1]

[1] Division of Life Sciences, Graduate School of Kyoto Sangyo University, Motoyama, Kamigamo, Kita, Kyoto 603-8555

[2] CRIA, Kyoto University 606-8507

Corresponding author: Nobuhiro Nakamura, Division of Life Sciences, Graduate School of Kyoto Sangyo University, Motoyama, Kamigamo, Kita, Kyoto 603-8555

+81-75-705-3018 osaru3@cc.kyoto-su.ac.jp

Running Title: Regulation of YIPFα1A expression at multiple levels

Abbreviations: YIPF; Yip domain family, UTR; untranslated region, CAI; codon adaptation index, s.d.; standard deviation, s.e.m.; standard error of the mean, CMV; cytomegalovirus, SV40; simian virus 40, poly(A) signal; polyadenylation signal, HA; hemagglutinin, GAPDH; glyceraldehyde-3-phosphate dehydrogenase

Key words: Golgi, complex formation, mRNA stability, codon adaptation index, 3′ untranslated region, [ER, translation, gene expression, transmembrane protein, poly(A)]

Conflicts of interest: none

Summary

YIPF is a family of five-span transmembrane proteins primarily localized at the Golgi apparatus. A YIPF α-subunit associates with a specific β-subunit partner to form a dimer, and the dimers further assemble into higher-order oligomers. The expression of an α-subunit partner is necessary for the efficient expression of its β-subunit partner. Curiously, conventional exogenous expression of α-subunits has proven extremely difficult, preventing further analysis of the YIPF complexes. To address this issue, the genetic information of YIPF was closely examined to determine why the exogenous expression of the YIPF α-subunits is inhibited. We identified two common features among YIPFs with poor exogenous expression: (1) the coding sequences of the YIPF α-subunits are enriched with rare codons, and (2) their mRNAs possess extended 3′ untranslated regions (UTRs). Our experimental evaluation of these features, focusing on YIPFα1A, revealed that both significantly influence YIPFα1A protein expression. First, the enrichment of rare codons markedly reduced YIPFα1A expression notably at the mRNA level. Second, the 3′ UTR of YIPFα1A was found to enhance its expression at the mRNA level. The deletion analysis revealed that the proximal region of the 3′ UTR, adjacent to the coding sequence, plays a key role in increasing mRNA abundance.

Introduction

The Golgi apparatus is a central organelle in the secretory pathway. Newly synthesized secretory and transmembrane proteins in the endoplasmic reticulum (ER) are transported to the Golgi apparatus, where they undergo processing, sorting, and are subsequently directed to their final destinations, such as the lysosome, plasma membrane, or extracellular space. The primary functions of the Golgi apparatus include the synthesis and modification of glycan chains, sulfation of amino acid side chains and glycans, and proteolytic cleavage that matures transit proteins [1–4] .

In vertebrates, including mammals, the Golgi apparatus exhibits a stacked cisternal structure [5] . The enzymes responsible for protein processing are distributed in a polarized manner: early-acting enzymes are concentrated at the *cis* side (entry), while late-acting enzymes are concentrated at the *trans* side (exit) [6,7] . Over the past half-century, the molecular mechanisms governing vesicular transport from the ER, through the Golgi apparatus, and to final destinations have been extensively studied [8] . This body of research was recognized with the Nobel Prize in Physiology or Medicine in 2013 [9,10] .

In parallel, the mechanisms underlying the localization of Golgi membrane proteins—particularly those involved in protein glycosylation—have also been investigated, revealing significant details [9,10] . However, the precise molecular mechanisms that maintain the polarized localization of Golgi proteins remain elusive [6,7] . Our research has focused on elucidating the molecular mechanisms that maintain Golgi structure and protein localization, specifically through the interactions between peripheral membrane

proteins—such as GM130 and GRASP65—and integral transmembrane proteins [11–15] .

During the course of our studies, we became interested in a family of multi-span transmembrane proteins, now referred to as YIP domain family (YIPF) proteins, which may serve as an interface between peripheral and integral Golgi membrane proteins [16]. YIPF proteins are a family of five-span transmembrane proteins primarily localized to the Golgi apparatus and conserved across the eukaryotic kingdom [16]. Yip1p and Yif1p are the founding members of YIPF proteins originally identified in budding yeast *Saccharomyces cerevisiae* [17,18] . They are essential for cell growth and are proposed to function in the fusion of ER-derived transport vesicle to the Golgi apparatus in association with Rab/Ypt family small GTPases [17,18]. Later studies revealed that these proteins are also involved in vesicle budding at the ER; however, whether they directly participate in vesicle budding itself or confer fusion competency to the target membrane remains controversial [19–21]. In addition to Yip1p and Yif1p, budding yeast possesses two paralogues, Yip4p and Yip5p, which are non-essential and whose functions remain unknown [17,18,22,23].

Over two decades of research, we have uncovered fundamental molecular characteristics of YIPF proteins. (1) Nine family members exist in humans and other mammals. These are classified into two subgroups, represented by the yeast proteins Yip1p and Yif1p. One member from each subgroup forms a dimer in a specific pairing. Furthermore, two to four dimers assemble to form higher-order complexes [24–26]. (2) They form three distinct complexes with overlapping distributions: the YIPF1 complex localizes mainly to the ER-Golgi intermediate compartment (ERGIC), the YIPF2

complex to the *cis*-Golgi, and the YIPF3 complex to the *trans*-Golgi. Based on these features, we previously categorized the Yip1p subgroup as α-subunits and the Yif1p subgroup as β-subunits, renaming each YIPF member according to its complex localization and subgroup designation [16]. (3) The expression of β-subunit depends on that of α-subunit, as knockdown of α-subunit also reduces the expression of its β-subunit partner. (4) The YIPF1 and YIPF2 complexes play roles in maintaining Golgi structure, whereas the YIPF3 complex is involved in proper glycosylation [24–26].

During our research, we observed that most YIPF α-subunits were poorly expressed in standard transient expression systems using conventional plasmid expression vectors that carry only the coding sequence. The expression was poor even under strong promoter systems such as cytomegalovirus (CMV) promoter and the human elongation factor 1α-subunit (hEF-1α) promoter. This poor expression impeded further analysis of YIPF complexes. We therefore sought to determine why YIPF α-subunits were so poorly expressed. Careful inspection of YIPF genetic information revealed two common features among poorly expressed YIPF α-subunits. One feature is the enrichment of rare codons in their coding sequences. The other is the presence of extended 3′ untranslated regions (UTRs) in their mRNAs. Experimental analyses confirmed that these two features play significant roles in regulating YIPFα1A expression. Specifically, the enrichment of rare codons in YIPFα1A markedly reduced its protein expression. Conversely, the 3′ UTR of YIPFα1A enhanced its expression. Deletion analysis revealed that the 3′ UTR adjacent to the coding sequence is necessary and sufficient to enhance YIPFα1A expression at the mRNA level. The significance of these regulatory mechanisms at both the mRNA and translational levels is discussed.

Results

Differential expression levels among YIPF family members

To begin the analyses, the exogenous expression of all YIPF family proteins was compared by inserting their coding sequences into CMV promoter-based expression plasmids with an N-terminal HA epitope tag. As shown in Fig. 1, we successfully expressed all YIPF proteins in HEK293 cells. However, expression levels varied significantly among constructs. To evaluate statistical significance, quantitative analysis of expressed proteins was performed. Due to the large dynamic range, direct comparison of all samples was not feasible; therefore, samples were divided into three sets and analyzed as ratios, as shown in Fig. 1B.

To minimize background signal interference, a narrow quantification area was selected for samples with lower signals (YIPFα1A, YIPFα1B, YIPFα2, YIPFα3, YIPFβ1A, YIPFβ1B; areas indicated by red lines on the left of the lanes). For samples with higher signals, a broader area was selected to include post-translationally modified forms (YIPFβ1B, YIPFβ2, YIPFβ3A, YIPFβ3B; areas indicated by red lines on the right of the lanes). Statistical analysis revealed that expression levels were significantly different between samples, with the exception of YIPFα1B vs. YIPFα2 and YIPFβ3A vs. YIPFβ3B comparisons (Fig. 1B).

To integrate results across the three sets, YIPFα1B and YIPFβ1B values served as reference points (Fig. 1C). The integrated results demonstrated that α-subunit expression levels were consistently low, while β-subunit expression was generally high (except for YIPFβ1A and YIPFβ1B). Notably, YIPFα1A and YIPFα3 showed

extremely low expression levels, approximately less than 1/700th that of YIPFβ3A or YIPFβ3B. Since all YIPF coding sequences were expressed under identical promoter and terminator control, the observed differences in protein expression levels can be attributed to intrinsic properties of the respective coding sequences.

Genetic characteristics of YIPF proteins

To investigate why some YIPF proteins are poorly expressed, the genetic information of YIPF proteins was thoroughly examined. We identified two common features among YIPF α-subunits (Table I). One of these features was a lower codon adaptation index (CAI) [27]. As summarized in Table I, CAI values were below 0.7 for most α-subunits (YIPFα1A, YIPFα2, and YIPFα3), whereas β-subunits showed CAI values exceeding 0.7. The lower CAI value indicates an enrichment of rare codons, that is predicted to reduce the translation efficiency of their coding sequences [28]. Another common feature of YIPF α-subunits was the presence of extended 3′ UTRs in their mRNAs (Table I). It has been reported that the 3′ UTR modulates protein expression by stabilizing or destabilizing the transcript and/or influencing translation efficiency [29–31]. The 3′ UTR has also been reported to direct transcript localization to specific subcellular compartments, thereby restricting the site of translation and/or facilitating interactions between nascent proteins and other cellular components. These processes ultimately influence translation efficiency and protein function [29–31] . Because the 3′ UTR was omitted in the conventional exogenous expression experiments (Fig. 1), its removal may have contributed to reduced protein expression. Hereafter, we focused on YIPFα1A to evaluate the impact of rare codon enrichment and the extended 3′ UTR on protein expression.

Codon usage affects YIPFα1A expression

The codon adaptation index (CAI) of wild-type (WT) YIPFα1A is 0.67. Notably, 43 codons in its coding sequence are rare (<16%) according to the human codon usage table [27,32]. To assess the impact of rare codon enrichment, we replaced all 43 rare codons with higher-frequency codons to generate a codon-optimized mutant (Table II, CAI = 0.84). Both the wild-type and codon-optimized mutants were tagged with N-terminal HA epitope to distinguish exogenous proteins from endogenous ones and were expressed in HEK293 cells as previously described.

Wild-type YIPFα1A protein (WT) expressed exogenously was barely detectable by anti-HA antibody, even with extended exposure times (Fig. 2A, left lower panel; arrowhead on the right), and remained below the detection threshold for anti-YIPFα1A antibody (Fig. 2A right lower panel, arrowhead on the right). These results indicate that exogenous YIPFα1A protein expression from the wild-type coding sequence is extremely low compared to the expression of the endogenous protein. In contrast, exogenous protein expression was markedly improved following codon optimization (Fig. 2A; Op) allowing detection by anti-YIPFα1A antibody. Quantitative analysis showed that the amount of the exogenously expressed protein was approximately four times greater than the endogenous protein (Fig. 2B). The amount of exogenously expressed protein from codon-optimized YIPFα1A was approximately 30-fold higher than that of the wild-type (WT), as measured by anti-HA antibody (Fig. 2C). Thus, the amount of exogenously expressed YIPFα1A protein from the wild-type coding sequence was estimated to be approximately one-eighth the amount of the endogenously expressed YIPFα1A protein. These results demonstrate that the inefficient expression of

YIPFα1A is primarily due to the enrichment of rare codons in its coding sequence.

YIPFα1A expression was increased at the mRNA level by codon optimization

Enrichment of rare codons was thought to cause inefficient translation of the mRNA, resulting in low protein synthesis. On the other hand, recent studies have demonstrated that rare codon enrichment can induce translation-mediated mRNA decay, thereby reducing protein expression even at the mRNA level [33,34]. To assess the impact of rare codon enrichment in the YIPFα1A coding sequence on mRNA abundance, northern blotting was performed using an RNA probe targeting the HA tag (Fig.2 D) or the coding sequence of YIPFα1A (Fig. 2F). As expected, both wild-type and codon-optimized mutant showed a single major band of expected size (approximately 1.1 kb) with either of probes. However, mRNA levels were markedly increased in the codon-optimized mutant compared to the wild-type (Fig. 2D). The increase was approximately 30-fold relative to the wild-type (Fig. 2E), similar to that observed at the protein level (Fig. 2C). These results suggest that the poor exogenous expression of YIPFα1A is primarily due to reduced mRNA levels.

Two major bands (2.0 kb and 3.2 kb) were detected by the coding sequence probe of YIPFα1A in non-transfected control cells (Fig. 2F; heavy, N). This result indicated that there are two isoforms of endogenous mRNAs for YIPFα1A in HEK293 cells, consistent with our previous experiments showing that most human tissues express two similarly sized transcript variants [35] . The exogenous expression of wild-type YIPFα1A mRNA was relatively higher than endogenous mRNA expression (Fig. 2F; N vs. WT). Quantitative analysis of the major band of wild-type YIPFα1A mRNA expressed exogenously and the sum of the endogenously expressed two differently sized

mRNA species showed that the exogenous expression was approximately 20-fold higher than endogenous expression (Fig. 2G). This result was in strong contrast to the extremely low expression of exogenous YIPFα1A protein compared with endogenous protein (Fig. 2A-C), suggesting that protein expression from the endogenous YIPFα1A mRNA is significantly more efficient than that from exogenous mRNA.

3′ UTR enhances YIPFα1A expression

Because endogenous YIPFα1A mRNA showed much higher protein expression efficiency than exogenously expressed YIPFα1A mRNA lacking the 3′ UTR (Fig. 2), we predicted that the extended 3′ UTR−another common feature of poorly expressed α-subunits−would have a positive impact on YIPFα1A expression. Indeed, it has been reported that the 3′ UTR influences mRNA stability and/or localization, thereby regulating protein expression [29–31,36]. Therefore, the functional significance of the extended 3′ UTR of YIPFα1A was explored.

As described above, two isoforms of YIPFα1A mRNA were detected in HEK293 cells (Fig. 2F). The sizes of the larger (3.2 kb) and smaller (2.0 kb) transcripts corresponded well to the sizes of the full-length sequence (3395 bases) and the partial sequence up to the annotated internal poly(A) site (2284 bases) in the reference cDNA sequence of YIPFα1A (NM_001024947), respectively.

After confirming expression of YIPFα1A mRNA containing an extended 3′ UTR, we investigated the functional role of this 3′ UTR. For this purpose, a plasmid vector expressing YIPFα1A mRNA with its native, extended 3′ UTR was constructed (Fig. 3A, +). The constructs with (+) or without (−) the 3′ UTR were transfected into HEK293

cells, and YIPFα1A protein expression was compared by western blotting (Fig. 3B). Intriguingly, YIPFα1A protein expression was enhanced by the addition of the 3′ UTR (+ vs −). To eliminate the possibility that the inserted 3′ UTR DNA sequence affected transcription from the expression plasmid, and to control for transfection efficiency by equalizing plasmid size between experimental and control groups, two control constructs were designed. In these constructs, the 3′ UTR was inserted either upstream of the CMV promoter (Fig. 3A, −U) or downstream of the poly(A) signal (−D). In addition, restriction sites (AscI, SbfI) were introduced at both ends of the 3′ UTR to facilitate the construction of expression plasmids. As shown in Fig. 3C and D, the addition of the 3′ UTR (+R) clearly enhanced protein expression (approximately 2.5-fold) compared to the controls (−U, −D). These results strongly suggest that the 3′ UTR sequence plays a role in enhancing protein expression.

3′ UTR increased the expression of YIPFα1A mRNA.

Subsequently, northern blotting was performed to analyze the size (Fig. 3E) and quantity (Fig. 3F and G) of the exogenously expressed YIPFα1A mRNA from the construct containing the 3′ UTR (+R). In control samples lacking 3′ UTR (−, −U), one major band was detected at the estimated size of 1.1 kb (Fig. 3E; band 1). This size corresponds to the calculated transcript length from the control constructs (1052 bases). In contrast, three bands were detected in the construct containing the 3′ UTR (Fig. 3E; +R, bands 1–3). The estimated sizes of bands 1, 2, and 3 were 1.1 kb, 2.3 kb, and 3.4 kb, respectively. Band 3 was predicted to represent the fully transcribed mRNA terminated at the poly(A) signal at the 3′ end of the 3′ UTR (Fig. 3A; pA2), although the possibility that the signal might partially originate from transcripts extended to the

SV40 poly(A) signal could not be excluded (Fig. 3A; red arrow on the right of pA2). Band 2 was the most abundant (Fig. 3G) and was predicted to be the transcript terminated at the internal poly(A) signal (Fig. 3A; pA1). Detection of band 1 was somewhat unexpected, as no poly(A) signal corresponding to that transcript size was found. This was most likely a partial degradation product, and the possibility will be discussed further below. Importantly, mRNA levels were clearly increased in the presence of the 3′ UTR (Fig. 3G). These results strongly suggest that the 3′ UTR plays a role in enhancing YIPFα1A protein expression at the mRNA level.

Functional analysis of transcripts with longer and shorter 3′ UTR

As mentioned above, northern blotting analyses revealed that the exogenous expression of YIPFα1A with a 3′ UTR sequence produced larger and smaller mRNA isoforms whose sizes matched well with those of the endogenous mRNA. Therefore, the functional significance of the larger and smaller mRNA was explored. Initially, the actual poly(A) signal responsible for producing the smaller mRNA was determined by introducing mutations at candidate poly(A) signal sequences near the center of the 3′ UTR predicted to yield appropriately sized transcripts. Four candidate sequences were chosen and the last A in the signal was mutated to G, a change reported to abolish signal function (Table III, Δ3~6) [37]. As a result, only the Δ4 mutant showed a significant increase in the larger transcript with a concomitant decrease in the smaller transcript (Fig. 4A and B). This result clearly indicated that the sequence at positions 1104–1110 (AUUAAA), which is in fact the annotated internal poly(A) signal, is the true poly(A) signal responsible for producing the smaller transcript.

Interestingly, quantitation of the total mRNA (sum of larger and smaller transcripts)

revealed that the disruption of the internal poly(A) signal in the mutant (Δ4) did not influence the total amount of mRNA (Fig. 4C). In accordance with this, the expression of YIPFα1A protein was also not affected by the mutation (Fig. 4D and E). These results suggest that the smaller transcript, containing only the proximal region of the 3′ UTR, includes an element necessary for the increase in YIPFα1A expression.

Functional mapping of 3′ UTR regulatory elements

To confirm the function of the proximal region of the 3′ UTR, the 3′ UTR sequence was divided into proximal (1–1118) and distal (1116–2230) fragments immediately downstream of the internal poly(A) signal, which produced the smaller transcript (Fig. 3A; pA1). The fragments were inserted downstream of the coding sequence or into the control position to construct the expression plasmids and analyzed as before. Western blotting analysis revealed that the proximal fragment (1–1118), but not the distal fragment (1116–2230), increased YIPFα1A protein expression (Fig. 5A). This result was consistent with the prediction that the proximal region of the 3′ UTR includes an element necessary for enhancing YIPFα1A protein expression.

Northern blotting analysis showed that the mRNA level was increased by the addition of the proximal fragment to a level similar to that of the protein (Fig. 5B). However, the addition of the distal fragment also increased mRNA levels to a level similar to that of the proximal fragment. This result was somewhat unexpected, because the result obtained with the full-length 3′ UTR suggested that the increase in protein expression was due to elevated mRNA level (Fig. 3E). These results implied a regulatory function of the 3′ UTR at the post-transcriptional level: either the proximal region enhanced protein expression per mRNA molecule, or the distal region suppressed it. These

possibilities were evaluated by a subsequent deletion analysis, as described below.

Identification of a 3′ UTR region that enhances protein expression

Various deletion fragments of the 3′ UTR (Fig. 6B, left) were generated and inserted either downstream of the coding sequence (+) or into the control position (−; downstream of the SV40 poly(A) signal) to construct the expression plasmids and analyzed by western blotting as described above (Fig. 6A). The N-terminal HA-tag was replaced with a HiBiT-tag for efficient detection. Notably, protein localization within the cell was unaffected by the tag replacement (data not shown). Quantitation was performed as previously described, and the results are shown as fold increases in protein expression, calculated by dividing the amount of protein expressed from the construct containing the 3′ UTR fragment (+) by that from the corresponding control (−) (Fig. 6B).

All fragments containing the 3′ UTR region adjacent to the coding sequence (1‑373) increased YIPFα1A protein expression to similar levels (full, 1–1118, 1–746, 1–373). In contrast, all fragments lacking this region failed to do so (1116–2230, 374–1118, 374–746, 747–1118). These results clearly indicate that the 3′ UTR region adjacent to the coding sequence (1‑373) is necessary and sufficient to enhance YIPFα1A protein expression. In addition, expression was increased by the shortest fragment (1–200), but not by the control 3′ UTR of glyceraldehyde-3-phosphate dehydrogenase (GAPDH) of the same size. These results strongly suggest that a regulatory element responsible for enhancing YIPFα1A protein expression resides in the 3′ UTR region adjacent to the coding sequence (1‑200).

Identification of a 3′ UTR region that enhances mRNA expression

Next, mRNA expression was analyzed by northern blotting. As shown in Fig. 7A, mRNAs of expected sizes were detected for all constructs with 3′ UTR fragments and their controls. This result indicated that the attached 3′ UTR sequences were successfully transcribed along with the coding sequence. Then, a simple comparison of the amount of the full-length transcript (Fig. 7A; F) was performed following the same procedures used in Fig. 5B (Fig. 7B, left bar graph; F). For the full-length 3′ UTR fragment (1–2230) sample, two bands corresponded to the larger and smaller transcripts were separately quantitated and summed up. The results were expressed as fold increases in mRNA levels, calculated by dividing the amount of full-length transcript of the sample containing a 3′ UTR fragment (+) by that of the corresponding control (−). All fragments containing the 3′ UTR region adjacent to the coding sequence (1‑373) increased YIPFα1A mRNA expression to similar levels (full, 1–1118, 1–746, 1–373). In contrast, the fragments lacking this region did not (374–1118, 374–746, 747–1118), except for the distal fragment of 3′ UTR (1116–2230). As was the case for the protein increase, the mRNA level was also increased by the shortest fragment (1–200) but not by the control GAPDH 3′ UTR of the same size. These results strongly suggest that the 3′ UTR region adjacent to the coding sequence (1‑200) is responsible for the increase in YIPFα1A protein expression at the mRNA level.

Curiously, the distal fragment of 3′ UTR (1116–2230) increased mRNA levels but not protein levels as observed earlier (Fig. 5). Considering the clear function of the 3′ UTR region adjacent to the coding sequence (1‑200) in the correlated increase in mRNA and protein levels, the distal fragment of 3′ UTR (1116–2230) was suggested to reduce

protein levels, probably at the translational level. To investigate the function of the 3′ UTR in regulating protein expression independently of mRNA level increase, the increase in protein levels was compared with that of mRNA levels. For this purpose, the ratio of the increase in protein levels to the increase in mRNA levels was calculated (Fig. 8, left bar graph). Indeed, the distal fragment of 3′ UTR (1116–2230) showed a ratio less than 1.0, while the full-length and the proximal fragments of 3′ UTR (1–1118) showed a ratio greater than 1.0, supporting this interpretation. However, the ratios of other fragments were contradictory. Specifically, the ratio of 3′ UTR fragment (374–1118) was particularly high (about 2), while the front half of that fragment (374–746) showed a lower ratio than the whole fragment, and the rear half of that fragment (747–1118) showed the ratio even less than 1.0. These results raised questions about the credibility of the method used to compare protein and mRNA levels.

In Northern blotting, it was noticed that signals of smaller products were also detected for all constructs (Fig. 7A; S and D). As discussed earlier for the construct with full-length 3′ UTR (Fig. 3E), these transcripts were predicted to be degradation products of the fully transcribed mRNA of the expected size (Fig. 7A; F). The signals of these smaller products varied in size and intensity between constructs (Fig. 7A). In particular, there are significant product signals with equal or greater size than the complete full-length transcript of the control (Fig. 7A; S). Because the amount of protein analyzed by Western blotting reflected accumulation over 24 hours, the amount of complete full-length mRNA recovered at the same time point would not directly reflect the amount of mRNA contributed to protein synthesis. Thus, smaller products with sizes equal to or greater than the control's full-length transcript likely represented transcripts that had

just completed their role in protein synthesis and were undergoing degradation, and should be included in transcript quantitation. Additionally, considering the difference in mRNA quality depending on the attached 3′ UTR fragments, the mRNA quantitation method was revised as follows.

Each lane was divided into three areas: (1) an area containing the full-length transcript (F; main); (2) an area containing transcripts smaller than the full-length but equal to or larger than the control's full-length transcript (S; smaller); and (3) an area containing transcripts smaller than the control's full-length transcript, likely representing degradation products (D; degraded). Quantitation of each area was performed as described in the Methods, and the percentage ratios of signal intensities in the three areas for each sample were calculated (Fig. 7B, right bar graph). In parallel, the amount of the transcripts equal to or larger than control's full-length transcript (F+S) was compared. The results were presented as an increase in mRNA levels (Fig. 7B, left bar graph, F+S).

The ratios of the amounts in the three areas varied among the 3′ UTR fragments (Fig. 7B, right), but interestingly, a negative correlation was observed between the amount of the full-length transcript (F) and that of the degradation product (D). Specifically, for the full-length, 1–1118, 1–746, 1–373, and 1–200 fragments of the YIPFα1A 3′ UTR, the amount of the full-length transcript was higher, and that of the degradation product was lower. Conversely, for the 374–1118, 374–746, 747–1118 fragments of the YIPFα1A 3′ UTR, the amount of the full-length transcript was lower, and that of the degradation product was higher. This negative correlation suggested that the full-length transcript was increased by the reduction in degradation. Notably, for the 1116–2230

fragment, the amount of the full-length transcript was similar to that of the 1–1118 fragment, but the amount of the degradation product was also higher. Similar results were observed for the GAPDH 3′ UTR. The significance of these differences remains unclear, but it may be attributed to faster clearance of the smaller products (S) that contain the 1116–2230 fragment of the YIPFα1A 3′ UTR.

Using the revised method, the increase in mRNA levels was similar to that quantitated from the full-length transcript alone, but became significantly higher for several fragments, notably the full-length 3′ UTR, 1–1118, 1116–2230, 1–746, and 374–1118 fragments of the YIPFα1A 3′ UTR (Fig. 7B, left bar graph; F+S). When the ratio of the increase in protein levels to the increase in mRNA levels was calculated (Fig. 8, right bar graph), it was approximately 1.0 for most of the constructs including those with full-length, 1–1118, 374–1118, and 374–746 fragments of the YIPFα1A 3′ UTR. In contrast to the results obtained using only the full-length transcript, the revised method indicated that the 374–1118 region did not enhance protein expression per mRNA molecules. Thus, the revised method yielded more consistent and interpretable results, strongly suggesting that YIPFα1A protein expression is promoted at the mRNA level by the most proximal region (1–200) of the 3′ UTR.

Conversely, 3′ UTR fragments containing 1116–2230 and 747–1118 showed a ratio below 1.0 in both quantitation methods, suggesting these regions may contain elements that suppress protein expression per mRNA molecule, likely by reducing translational efficiency. However, the constructs with full-length 3′ UTR or the ΔpA4 mutant, which also include the 1116–2230 region, did not exhibit the same effect (Figs. 4 and 8). Furthermore, the 3′ UTR fragments 1–1118 and 374–1118, which encompass the 747–

1118 region, likewise did not show the same effect (Fig. 8). Therefore, the functional role of these regions remains inconclusive at present. Further detailed analysis will be necessary to evaluate this possibility.

Discussion

This study demonstrated that YIPFα1A protein expression is tightly regulated at multiple post-transcriptional levels. Firstly, protein expression was strongly repressed by the enrichment of rare codons in the coding sequence. This repression occurred primarily at the mRNA level, as codon optimization increased mRNA expression to a level comparable to that of protein expression (Fig. 2; approximately 30-fold). The repression of mRNA expression is thought to result from mRNA degradation induced by the enrichment of rare codons in the coding sequence, as reported previously [33,38–44]. In the transient expression system used in this study, the amount of protein accumulated in the cells correlates with that of mRNA levels, though not necessarily in a linear manner. Therefore, the observation that protein and mRNA levels increased similarly does not exclude the possibility of enhanced translation efficiency. This possibility should be tested in future studies examining mRNA translation efficiency by *in vitro* translation assay.

Secondly, the 3′ UTR was found to enhance the expression of YIPFα1A protein at the mRNA level (Figs. 3 and 5–7). It has been reported that longer 3′ UTRs are associated with greater mRNA stability [42]. Therefore, we hypothesized that extension of the 3′ UTR length, regardless of its sequence, would stabilize the mRNA and thereby increase both mRNA and protein levels (Fig. 3). However, regulation of mRNA stability and translation is influenced not only by length but also by multiple *cis*-regulatory elements within the 3′ UTR. *Cis*-regulatory elements can modulate mRNA abundance and final protein output by interacting with RNA-binding proteins (RBPs) or microRNAs (miRNAs), thereby either enhancing or repressing gene expression [31,34] . Indeed, the

most proximal fragment of the 3′ UTR (1–200) was sufficient to promote YIPFα1A expression at the mRNA level (Figs. 6 and 7). Thus, it is not the overall length of the 3′ UTR, but rather the presence of the proximal region (1–200) that promotes mRNA expression.

Interestingly, we observed products that were smaller than the full-length transcript but equal to or larger than the control transcript. The amounts of these products varied between constructs containing different 3′ UTR elements (Fig. 7B). We hypothesized that these smaller products represent partial degradation products that may have contributed to protein synthesis before cells were harvested for analysis. The protein-per-mRNA comparison results were more consistent and provided reasonable support for our hypothesis (Fig. 8). It is probable that different sets of RBPs bind to each construct and contribute to the observed differences in mRNA stability. However, we cannot exclude the possibility that these smaller products were incomplete or partial transcripts produced by an unknown mechanism. This alternative possibility will need to be evaluated by analyzing the stability of full-length transcripts in future studies.

How the proximal region (1‑200) of the 3′ UTR increases mRNA levels is another problem to be tackled in future studies. The reduction of degradation products from the construct with the proximal region (1‑200) of the 3′ UTR strongly suggests that this proximal region increases mRNA stability (Fig. 7A and B, right panel). mRNA stability is regulated through various mechanisms involving miRNAs, long noncoding RNAs, and RBPs, including enzymes that modify RNA [45]. The 3′ UTR is a major target of these regulatory mechanisms. Among RBPs, HuR is known to stabilize mRNA by binding to AU-rich elements in the 3′ UTR [46,47]. Notably, two AUUUA motifs are

found in the proximal region (1‑200) of the YIPF α 1A 3′ UTR. Evaluating the role of these motifs is clearly a priority for our future studies.

Interestingly, elements that repress translation may also reside within the 3′ UTR (747–1118, 1118–2230) (Fig. 8). This possibility is supported by reports that the 3′ UTR can repress translation via interaction with RBPs or miRNAs [48]. However, this effect was not observed when these regions were present alongside other segments (1–1118, 374–1118, or full-length); therefore, further detailed analysis is required to confirm the translational regulatory roles of these regions.

Thirdly, the existence of a mechanism facilitating efficient expression of endogenous YIPFα1A was suggested, as the expression of endogenous protein appeared to be substantially more efficient when comparing protein and mRNA levels (Fig. 2). When a construct containing the wild-type YIPFα1A coding sequence without the 3′ UTR was used, exogenously expressed mRNA levels were approximately 20-fold higher than endogenous mRNA levels (Fig. 2F and G). However, exogenously expressed protein levels were only approximately one-eighth of endogenous protein levels (Fig. 2A-C). Therefore, the amount of protein per mRNA was approximately 160-fold higher for endogenous mRNA than exogenous mRNA. Because the addition of full length 3′ UTR increased both mRNA and protein amounts to a similar extent (Fig. 3, approximately 2.5-fold), the presence of the 3′ UTR could not explain the large difference in protein expression efficiency per mRNA.

The primary difference between endogenous and exogenous gene expression appears to be the presence or absence of the co-expression of the β-subunit (YIPFβ1A or

YIPFβ1B). It is likely that the absence of β-subunit expression impairs translation of exogenously expressed mRNA or promotes degradation of excess YIPFα1A lacking a partner protein via the ER-associated degradation (ERAD) pathway [49] . These possibilities are currently being investigated using co-expression systems involving YIPFα1A and β-subunit (YIPFβ1A or YIPFβ1B).

As discussed above, the expression of β-subunits appears to be controlled with that of the α-subunits. Since YIPF proteins are five-span transmembrane proteins that form α/β dimers, the resulting complex contains ten transmembrane domains. The α-subunit must locate its specific β-subunit partner, avoiding non-specific interactions with unrelated β-subunits or other membrane proteins. Therefore, it is reasonable to assume that complex assembly is tightly regulated during synthesis in the endoplasmic reticulum (ER). However, mechanisms and sites of membrane protein complex formation and regulation remain poorly understood. From this perspective, reports indicating that the 3′ UTR plays a role in regulating ER export of membrane proteins, specifically at a specialized ER subdomain known as the TIGER domain [50,51] , suggest an intriguing hypothesis. This hypothesis posits that the synthesis and trafficking of YIPFα1A are regulated via the 3′ UTR and its interacting RBPs at a defined ER subregion, thereby facilitating correct dimerization with the β-subunits. To explore this possibility, we are now developing a method to evaluate *in situ* mRNA localization along with expressed protein.

Although it is outside the scope of this report, it should be noted that the 5′ UTR may also contribute to the regulation of YIPFα1A expression [52,53] . It is noteworthy that the human YIPFα1A gene encodes two mRNA isoforms with different 5′ UTR lengths.

The larger isoform (NM_0010297) contains 386 nucleotides, while the smaller isoform (NM_030799) contains 135 nucleotides in the 5′ UTR. The function of the 5′ UTR, in conjunction with the 3′ UTR, could be evaluated by adding or deleting the 5′ UTR in our experimental system.

Our findings have broader implications for understanding post-transcriptional regulation in eukaryotic cells. The multilayered control of YIPFα1A expression exemplifies how cells coordinate protein complex assembly, particularly for membrane proteins that must avoid misfolding and aggregation. The conservation of suboptimal codon usage among human YIPF α-subunits suggests this represents an evolutionarily maintained regulatory mechanism rather than neutral drift. The slower translation kinetics resulting from suboptimal codon usage likely facilitates proper co-translational folding and complex assembly while preventing protein aggregation [54]. These regulatory mechanisms have important practical implications for protein expression systems [55] . Our findings indicate that successful heterologous expression of membrane protein complexes may require not only codon optimization strategies but also preservation of native regulatory elements, particularly 3′ UTRs that control mRNA stability and translation efficiency.

The multilayered regulation of YIPFα1A expression suggests that YIPF complex formation may be dynamically modulated during development, cellular differentiation, and stress responses. This regulatory complexity likely reflects the critical requirement for precise YIPF complex stoichiometry in maintaining Golgi architecture and cellular homeostasis. Future investigations into these regulatory networks will provide crucial insights into fundamental membrane trafficking mechanisms and may illuminate disease

states involving Golgi dysfunction and aberrant YIPF protein function.

Methods

Reagents and Cell culture

All reagents were biochemical or molecular biology grade (Nacalai Tesque, Kyoto, Japan or FUJIFILM Wako Pure Chemical Corp., Osaka, Japan). Restriction enzymes were purchased (New England Biolabs, Ipswich, MA, USA, TAKARA Bio Inc., Shiga, Japan or TOYOBO Co. Ltd., Osaka, Japan). HEK293 cells were cultured in high glucose Dulbecco's Modified Eagle's Medium (DMEM) (FUJIFILM Wako) supplemented with 10% fetal bovine serum (Sigma-Aldrich Co., St. Louis, MO, USA) as a growth medium in humidified air with 5% CO_2 at 37˚C.

cDNA and Plasmid construction

We described cloning of YIPF protein cDNAs previously [35], except for YIPFα1B, which was purchased (Sino Biological Inc., Beijing, China). The cDNA sequence of the 3′ UTR of YIPFα1A and GAPDH was cloned by RT-PCR using a laboratory-made cDNA library. The poly(A) RNA was purified from HEK293 cells using MagExtractor RNA (TOYOBO) and Oligotex-dT30 <Super> mRNA Purification Kit (TAKARA Bio). It was reverse transcribed using PrimeScript II 1st Strand cDNA Synthesis Kit (TAKARA Bio) following the manufacturer's protocol. PCR was performed using deduced primers to amplify from the end of the coding sequence to the 3′ end of the longest cDNA sequence found in the database, excluding the poly(A) tail (YIPF1αA: NM_001024947, 2230 bp; GAPDH: BC083511, 200 bp). The sequence completely matched the database sequence. Native 3′ UTR sequence was reproduced by attaching to the YIPFα1A coding sequence using In-Fusion cloning (TAKARA Bio) following

the manufacturer's protocol. Full-length and deletion fragments of the 3′ UTR were produced by PCR using a pair of primers containing appropriate restriction sites (AscI, SbfI). Expression plasmid vectors were constructed by replacing the EGFP coding sequence on pEGFP-C1 (TAKARA Bio) with YIPF coding sequences, attaching an epitope tag at the N-terminus and restriction sites at N- (NheI) and C-terminus (XhoI) for ease of cloning. Restriction sites (AscI and SbfI) were also introduced into the expression plasmid vectors for inserting various fragments of the 3′ UTR at the 3′ end of the coding sequence (TCTAGA GGCGCGCC ACAT CCTGCAGG CTGATCATAATC), the 5′ of the CMV promoter (GATTCTGT GGCGCGCC ACAT CCTGCAGG ATAACCGTAT) or the 3′ of the SV40 poly(A) signal (GTATCTTAACGCG GGCGCGCC ACAT CCTGCAGG CGCGTAAA). Plasmid vector cloning was performed using QuikChange Site-Directed Mutagenesis (Agilent Technologies Inc., Santa Clara, CA, USA), In-Fusion HD cloning, or conventional restriction site cloning following the manufacturer's protocol. N-terminal HA-tag (MYPYDVPDY) or HiBiT-tag with a linker sequence (MVSGWRLFKKIS GGGG; Promega Corp., Madison, WI, USA) was attached in-frame with coding sequences, interrupted by the NheI site (GCTAGC; AS). The original C-terminal stop codon was removed and replaced with XhoI and XbaI sites (CTCGAGCTCTAGA; LEL) for previously described C-terminal tagging studies [35]. For transfection experiments, plasmids were purified using the Plasmid Plus Midi Kit (QIAGEN GmbH, Hilden, Germany). Codon optimization was performed by PCR using appropriate primers. Briefly, the coding sequence was divided into seven segments with overlaps of approximately 20 base pairs. Each segment was PCR-amplified using appropriate primers containing designed mutations (Table II). The segments were joined by

extension PCR, and the final fused product was cloned using terminal restriction sites (NheI and XhoI) and sequence verified.

Transfection and cell harvest

Cells were seeded 16 hours before transfection (2.0×10^5 cells/3.5 cm dish for protein analysis, 4.0×10^5 cells/5.0 cm dish for RNA analysis). Transfection was performed using FuGENE 6 (Promega) at 1 μg DNA, 3 μL reagent ratio for protein analysis, doubled for RNA analysis, according to the manufacturer's protocol. Twenty-four hours after the transfection, cells were scraped from the dish using a cell scraper (Sumitomo Bakelite Co., Ltd., Tokyo, Japan) in the presence of 1 mL growth medium on ice. The cell suspension was recovered in a 1.5 mL centrifuge tube, spun for 5 seconds at maximum speed at 4˚C to pellet the cells, and the supernatant was removed. The cells were washed by adding 1mL ice-cold Dulbecco's PBS and spun for 5 seconds at maximum speed at 4˚C three times for protein extraction or once for RNA extraction. For protein analysis, 50 μL of 4% SDS, 0.05M Tris-HCl (pH6.7) solution was added, vortex-mixed to detach cell pellet and sonicated using BIORUPTOR (Sonicbio Co., Ltd., Kanagawa, Japan) until solution was no longer viscous (5‑10 minutes with 20-second intervals every 20 seconds in ice-cold water bath). The protein concentration of the cell lysate was measured using the Pierce BCA Protein Assay Kit (Thermo Fisher Scientific Inc., Rockford, IL, USA). An equal volume of 0.02% BPB, 0.05 M Tris-HCl (pH6.7), 0.4 M sucrose, 0.2 M dithiothreitol was added, and the protein concentration was adjusted to 1.0 μg/μL using 1×SDS-PAGE sample buffer (2% SDS , 0.01% BPB, 0.025M Tris-HCl (pH6.7), 0.2M Sucrose, 0.1M dithiothreitol). Total RNA was extracted using the MagExtractor RNA (TOYOBO) or the RNeasy Plus Mini Kit

(QIAGEN) according to the manufacturer's protocol. RNA concentration was measured using a BioSpectrometer equipped with a μCuvette G1.0 (Eppendorf Vertrieb Deutschland GmbH, Wesseling-Berzdorf, Germany).

Western blotting

This was performed as described previously, using an anti-YIPFα1A (YIPF5) antibody and anti-HA antibody (16B12; Covance Research Products, Inc., Berkeley, CA, USA) [26]. A peroxidase-conjugated anti-mouse and anti-rabbit IgG (Jackson ImmunoResearch Labs. Inc., West Grove, PA, USA) and Immobilon Western Chemiluminescent HRP Substrate (EMD Millipore Corp., Burlington, MA, USA) were used for detection. Detection of HiBiT tag was performed using the Nano-Glo HiBiT Blotting System (Promega), according to the manufacturer's protocol.

Northern blotting

This was performed using classical agarose gel electrophoresis and capillary transfer by downward flow [56]. Briefly, 1 μg of total RNA was loaded along with 2 μL of Prestain Marker for RNA High (BioDynamics Laboratory Inc., Tokyo, Japan) onto a 1% agarose gel containing formaldehyde and 1× MOPS electrophoresis buffer and run at 100 V for 50 minutes using a Mupid-2X (Mupid Co., Ltd., Tokyo, Japan). The RNA was transferred onto a positively charged nylon membrane (Roche Diagnostics GmbH, Mannheim, Germany) for 4 hours using alkaline transfer buffer. The membrane was UV-irradiated for 2 minutes and subjected to hybridization and detection using a DIG-labeled probe, DIG Easy Hyb, DIG Wash and Block Buffer Set and Anti-Digoxigenin-AP Fab fragments (Roche Diagnostics), following the manufacturer's protocol.

RNA probe synthesis

RNA probes were synthesized using DIG RNA Labeling Kit (Roche Diagnostics) with PCR amplified templates. As templates for PCR, plasmids containing the HA-tag only, HA-tagged YIPFα1A coding sequence and human β-actin coding sequence were constructed by inserting them between HindIII (AAGCTT CCACC ATG-HA-tag-coding) and XbaI (coding-CTCGAG C TCTAGA; LEL and stop codon) sites of pcDNA3 (Invitrogen, Thermo Fisher Scientific, Waltham, MA, USA). The YIPFα1A coding sequence with the HA tag, HA tag only (TAATACGACTCACTATAGGG AGACCCAAGCTTCCACC ATGTACCCCTACGACGTGCCCGACTACGCT AGAGGGCCCTATT CTATAGTGTCACCTAAAT; under lines indicate T7, HA tag, and SP6), and the target sequences were amplified by PCR using T7 and SP6 primers, and used for probe synthesis with SP6 primer.

Chemiluminescence image detection and quantitation

Chemiluminescent images were taken using the ImageQuant LAS4000 mini (GE Healthcare Technologies Inc., Chicago, IL, USA). Quantitation of images was performed using ImageJ [57] with TIFF-formatted files exported from the image analyzer. For the comparison of signal strength of bands from western blotting and northern blotting, each band of interest was manually selected using a fixed-size rectangle (areas are indicated in figures), and the mean grayscale intensity was recorded. The grayscale intensity of each band was normalized by subtracting the background, which was the mean grayscale intensity of three background areas. To calculate the mean across experiments, the ratio of the grayscale intensity of each band to the sum of grayscale intensities of all bands was calculated in each experiment. Then,

the mean, s.d. and s.e.m. of the ratio were calculated for each band, and these were further divided by the mean value of the standard to calculate the relative ratio. For the quantitation of the ratio (%) of differently sized products in northern blotting, the image was placed horizontally, and the lane of interest was manually selected using a rectangle. Then a profile of grayscale intensity was plotted, and the grayscale intensity values at each location on the blot were exported to an Excel file using the Plot Profile command. By consulting the image, the boundaries of main, sub and degradation areas were manually determined as indicated in Fig. 7A. The grayscale intensities of each area were summed, and the background was subtracted. The value of each area was divided by the total value of the three areas to calculate the ratio (%). The amount of the products that were equal to or larger than the control's full length product band (F+S) was quantitated in a similar way for the full length band quantitation, except that a larger area was selected, as indicated in Fig. 7A. An equal-size area was used for the control lane for comparison. For the calculation of the fold increase in Fig.7 and 8, the fold increase values were calculated for each experiment, and those values were used to calculate the mean, s.d. and s.e.m. For the calculation of s.d. and s.e.m. values in the three-set integration (Fig. 1) and the protein-to-mRNA ratio analysis (Fig. 8), standard propagation of uncertainty formulas was applied. Statistical analysis was performed using Statmate V (Atms Co. Ltd., Tokyo, Japan).

Author contributions

N.N. conceived and supervised the research project. T.T., Y.N., and N.N. conducted the experiments. N.N. prepared the manuscript.

Acknowledgements

We would like to thank Professors Yuichiro Mishima and Toshiya Endo for their contributions as assistant supervisors for TT and YN and critically reading the manuscript. We also thank Drs. Shin'ichiro Yoshimura, Akihiro Harada, Toru Yoshihisa, and Hiderou Yoshida for their valuable discussions and insightful comments. Finally, we are grateful to both past and present members of our laboratory for their contributions. This work was supported by the annual research allowance and a research grant from Kyoto Sangyo University (E2511).

Figure Legends

Figure 1. Exogenous expression efficiency of YIPF proteins

HEK293 cells were transfected with expression plasmids containing N-terminally HA-tagged YIPF protein cDNAs and analyzed by Western blotting after 24 hours using anti-HA antibody. (A) Representative Western blot showing equal protein loading (10 μg per lane) from three independent experiments. Molecular weight markers are indicated on the left. The bottom panel shows a longer exposure of the upper panel. White and black arrowheads indicate weak signals for YIPFα1A and YIPFα3, respectively. Red lines indicate the areas used for quantitation. (B) Quantitative analysis and statistical comparison of protein expression ratios within three separate sets. Statistical significance was determined using one-way ANOVA followed by Fisher's LSD (Least Significant Difference) test. Statistical significance: *$p < 0.05$, **$p < 0.01$, ns = not significant. (C) Integrated quantitative results from (B). Values from the middle panel in (B) were multiplied by the corresponding YIPFα1B value from the upper panel. Values from the lower panel in (B) were further multiplied by the YIPFβ1B value from the middle panel (which had already been normalized to YIPFα1B). Data represent mean ± s.e.m. (upper error bars) and ± s.d. (lower error bars); n = 3 independent experiments.

Figure 2. Codon optimization enhances YIPFα1A expression

HEK293 cells were transfected with N-terminally HA-tagged wild-type (WT) or codon-optimized (Op) YIPFα1A expression plasmids and analyzed after 24 hours by western blotting (A–C) or northern blotting (D–G). N: non-transfected control. Molecular weight markers (western blots) and size markers (northern blots) are shown on the left.

Red lines indicate the areas used for quantitation. All quantitation data represent mean ± s.e.m. (upper error bars) and ± s.d. (lower error bars); n = 3 independent experiments. (A) Western blot analysis using anti-HA (left) or anti-YIPFα1A (right) antibodies. Representative images from three experiments are shown; bottom panels show longer exposures. Arrows: endogenous YIPFα1A protein; arrowheads: exogenous HA-tagged YIPFα1A protein. (B) Quantitation of endogenous (endo) versus exogenous (exo) YIPFα1A protein levels from anti-YIPFα1A blots in (A, right panel). (C) Quantitation of wild-type versus codon-optimized YIPFα1A protein levels from anti-HA blots in (A, left panel). (D) Northern blot analysis of total RNA (1 μg per lane) using DIG-labeled probe detecting the HA tag. Light (left) and heavy (right) exposures of the same blot are shown. Arrow indicates expressed YIPFα1A mRNA. Representative image from three experiments. (E) Quantitation of total YIPFα1A mRNA levels from (D). (F) Northern blot analysis of total RNA (1 μg per lane) using DIG-labeled probe spanning the entire YIPFα1A coding sequence. Light (left) and heavy (right) exposures of the same blot are shown. Arrowheads: endogenous YIPFα1A mRNA; arrow: exogenous YIPFα1A mRNA. Representative image from three experiments. (G) Quantitation of exogenous YIPFα1A mRNA relative to the sum of endogenous YIPFα1A mRNA isoforms (larger and smaller forms) from (F). Statistical significance was determined by student T test (** $p < 0.01$, *** $p < 0.001$)

Figure 3. The expression of YIPFα1A was increased by the 3′ UTR

HEK293 cells were transfected with YIPF α 1A expression constructs containing different 3′ UTR configurations and analyzed by western and northern blotting. Molecular weight markers (western blots) and size markers (northern blots) are shown

on the left. Red lines indicate the areas used for quantitation. All quantitation data represent mean ± s.e.m. (upper error bars) and ± s.d. (lower error bars); n = 3 independent experiments. (A) Schematic representation of expression constructs. (−): coding sequence only; (+): native 3′ UTR directly connected to coding sequence; (+R): 3′ UTR with introduced restriction sites (AscI and SbfI, shown in green); (−U): 3′ UTR inserted upstream of CMV promoter; (−D): 3′ UTR inserted downstream of SV40 poly(A) signal. Red arrows indicate poly(A) signals: pA1 and pA2 within the YIPFα1A 3′ UTR, and SV40 poly(A). Predicted transcript regions for construct (+R) are shown below (bands 1, 2, and 3). (B, C) Representative western blots from three experiments. Arrowheads indicate YIPFα1A protein. (D) Quantitation of YIPFα1A protein levels relative to control (−U). (E) Representative northern blot using DIG-labeled probe spanning the entire YIPFα1A coding sequence showing three major transcript bands (1, 2, and 3, indicated by arrowheads). β-actin control blot using DIG-labeled probe spanning the entire β-actin coding sequence for the same samples is shown below. Red lines indicate quantified regions. (F) Relative abundance (%) of transcript bands 1, 2, and 3. (G) Total mRNA expression from 3′ UTR-containing construct (+R) relative to control (−). For (+R) samples, bands 2 and 3 were combined for quantitation. Statistical significance was determined using one-way ANOVA followed by Fisher's LSD test. (* $p < 0.05$, ** $p < 0.01$, ns = not significant).

Figure 4. Functional role of internal poly(A) signals in the YIPFα1A 3′ UTR

HEK293 cells were transfected with YIPFα1A expression constructs containing mutations in candidate poly(A) signals (Δ3–Δ6) within the 3′ UTR and analyzed by

northern and western blotting. Molecular weight markers (western blots) and size markers (northern blots) are shown on the left. Red lines indicate the areas used for quantitation. All quantitation data represent mean ± s.e.m. (upper error bars) and ± s.d. (lower error bars); n = 3 independent experiments. (A) Representative northern blot using DIG-labeled probe spanning the entire YIPFα1A coding sequence showing larger (L) and smaller (S) mRNA isoforms (indicated by arrowheads). (B) Percentage of larger-form mRNA expressed from each construct. (C) Relative YIPFα1A total mRNA levels (larger plus smaller isoforms combined) expressed from each construct compared with wild-type (WT). (D) Representative western blot showing YIPFα1A protein levels. Arrowhead indicates YIPFα1A protein; asterisk indicates non-specific signal. (E) Relative YIPFα1A protein levels expressed from each construct compared with wild-type (WT). Statistical significance was determined using one-way ANOVA followed by Fisher's LSD test. Statistical significance: **p < 0.01; no mark = not significant.

Figure 5. Functional analysis of proximal and distal regions of the YIPFα1A 3′ UTR

HEK293 cells were transfected with constructs containing YIPFα1A coding sequence and either proximal (1‑1118) or distal (1116‑2230) halves of the 3′ UTR. Constructs were designed with the 3′ UTR fragments either at the 3′ end of the coding sequence or at the control position (upstream of CMV promoter; −U from Fig. 3A). Molecular weight markers (western blots) and size markers (northern blots) are shown on the left. Red lines indicate the areas used for quantitation. All quantitation data represent mean ± s.e.m. (upper error bars) and ± s.d. (lower error bars); n = 3 independent experiments. (A) Western blot analysis of YIPFα1A protein expression (upper panel) and

quantitation (lower panel). Arrowhead indicates YIPFα1A protein; asterisk indicates non-specific signal. (B) Northern blot analysis of mRNA expression using DIG-labeled probe spanning the entire YIPFα1A coding sequence (upper panel) and quantitation (lower panel). Arrowhead 1: mRNA containing coding sequence only; arrowhead 2: mRNA containing coding sequence plus 3′ UTR fragment. Statistical significance was determined using one-way ANOVA followed by Fisher's LSD test. Statistical significance: * $p < 0.05$, ** $p < 0.01$; no mark = not significant.

Figure 6. Identification of 3′ UTR regions affecting protein expression

HEK293 cells were transfected with constructs containing YIPFα1A coding sequence (HiBiT-tagged) and various fragments of the YIPFα1A 3′ UTR or GAPDH 3′ UTR. Fragments were positioned either at the 3′ end of the coding sequence (+) or at the control position (−; downstream of SV40 poly(A) signal; −D from Fig. 3A). Molecular weight markers are shown on the left. Red lines indicate the areas used for quantitation. All quantitation data represent mean ± s.e.m. (right error bars) and ± s.d. (left error bars); n = 3 independent experiments. (A) Representative Nano-Glo chemiluminescence image showing YIPFα1A protein expression. Arrowhead indicates YIPFα1A protein. Fragment boundaries (numbers indicate nucleotide positions of 5′ and 3′ ends) are indicated at the top. (B) Quantitation and schematic summary. (Left) Schematic representation of 3′ UTR deletion constructs showing poly(A) signal positions (pA1, pA2; red arrows) and fragment boundaries. (Right) Fold increase in YIPFα1A protein expression calculated by dividing expression from constructs with 3′ UTR fragments (−) by corresponding controls (+). Red line indicates no change (ratio = 1). Statistical significance was determined by student T test (* $p < 0.05$, ** $p < 0.01$, *** $p < 0.001$,

ns = not significant).

Figure 7. Identification of a 3′ UTR region affecting mRNA expression

Northern blot analysis of constructs described in Figure 6. Size markers are shown on the left. Red lines with letters (F, S, D) indicate the areas used for quantitation. All quantitation data represent mean ± s.e.m. (right error bars) and ± s.d. (left error bars); n = 3–4 independent experiments. (A) Representative northern blot using DIG-labeled probe spanning the entire YIPFα1A coding sequence showing mRNA expression patterns for different 3′ UTR constructs. (B) Quantitation and analysis. (Left) Schematic representation (same as Fig. 6B). (Left bar graph) Fold increase in mRNA expression. F: quantitation of full-length transcript only; F+S: quantitation including full-length plus smaller products. Red line indicates no change (ratio = 1). (Right bar graph) Relative abundance of mRNA products in three size categories (F, S, D) for each construct. Statistical significance was determined by student T test (* $p < 0.05$, ** $p < 0.01$, *** $p < 0.001$, ns = not significant). Statistical significance of signal ratios between constructs is shown in Table IV.

Figure 8. Protein-to-mRNA expression ratio analysis

Analysis of protein expression enhancement relative to mRNA expression enhancement using data from Figures 6 and 7. All quantitation data represent mean ± s.e.m. (right error bars) and ± s.d. (left error bars) calculated according to the standard propagation of uncertainty formulas. (Left) Schematic representation of 3′ UTR deletion constructs (same as Figs. 6, 7). (Left bar graph) Protein/mRNA ratio calculated using full-length transcript only. (Right bar graph) Protein/mRNA ratio calculated including smaller

transcripts. Red line indicates no change (ratio = 1).

References

1 Warren G & Rothman J (eds.) (2011) *The Golgi* Cold Spring Harbour Laboratory Press, New York.

2 James M & H. M Hilton (2009) *The Golgi apparatus: The First 100 Years* Springer Science+Business, LLC, New York.

3 Mirronov, Alexsander, Pavelka & Margit (eds.) (2008) *The Golgi apparatus: State of art 110 years after Camillo Golgi's discovery* Springer-Verlag, Wien.

4 Berger EG & Roth J (eds.) (1997) *The Golgi apparatus* Springer Basel AG, Basel.

5 Klumperman J (2011) Architecture of the mammalian Golgi. *Cold Spring Harbor Perspectives in Biology* **3**, a005181.

6 Lujan P & Campelo F (2021) Should I stay or should I go? Golgi membrane spatial organization for protein sorting and retention. *Arch Biochem Biophys* **707**, 108921.

7 Banfield DK (2011) Mechanisms of protein retention in the Golgi. *Cold Spring Harbor Perspectives in Biology* **3**, a005264.

8 Bonifacino JS & Glick BS (2004) The mechanisms of vesicle budding and fusion. *Cell* **116**, 153–166.

9 Schekman R & Südhof T (2014) An interview with Randy Schekman and Thomas Südhof. *Trends in Cell Biology* **24**, 6–8.

10 Rothman JE (2014) The principle of membrane fusion in the cell (Nobel lecture). .

11 Yoshimura S, Nakamura N, Barr FA, Misumi Y, Ikehara Y, Ohno H, Sakaguchi M & Mihara K (2001) Direct targeting of cis-Golgi matrix proteins to the Golgi apparatus. *J Cell Sci* **114**, 4105–4115.

12 Nakamura N, Wei J-H & Seemann J (2012) Modular organization of the mammalian Golgi apparatus. *Curr Opin Cell Biol* **24**, 467–474.

13 Nakamura N (2010) Emerging new roles of GM130, a cis-Golgi matrix protein, in higher order cell functions. *J Pharmacol Sci* **112**, 255–264.

14 Lowe M, Nakamura N & Warren G (1998) Golgi division and membrane traffic. *Trends in Cell Biology* **8**, 40–44.

15 Barr FA, Nakamura N & Warren G (1998) Mapping the interaction between GRASP65 and GM130, components of a protein complex involved in the stacking of Golgi cisternae. *The EMBO journal* **17**, 3258–3268.

16 Shaik S, Pandey H, Thirumalasetti SK & Nakamura N (2019) Characteristics and Functions of the Yip1 Domain Family (YIPF), Multi-Span Transmembrane Proteins Mainly Localized to the Golgi Apparatus. *Frontiers Cell Dev Biology* **7**, 130.

17 Yang X, Matern HT & Gallwitz D (1998) Specific binding to a novel and essential Golgi membrane protein (Yip1p) functionally links the transport GTPases Ypt1p and Ypt31p. *The EMBO journal* **17**, 4954–4963.

18 Matern H, Yang X, Andrulis E, Sternglanz R, Trepte H-H & Gallwitz D (2000) A novel Golgi membrane protein is part of a GTPase-binding protein complex involved in vesicle targeting. *The EMBO journal* **19**, 4485–4492.

19 Heidtman M, Chen CZ, Collins RN & Barlowe C (2003) A role for Yip1p in COPII vesicle biogenesis. *The Journal of Cell Biology* **163**, 57–69.

20 Tang BL, Ong YS, Huang B, Wei S, Wong ET, Qi R, Horstmann H & Hong W (2001) A membrane protein enriched in endoplasmic reticulum exit sites interacts with COPII. *The Journal of biological chemistry* **276**, 40008–40017.

21 Barrowman J, Wang W, Zhang Y & Ferro-Novick S (2003) The Yip1p.Yif1p complex is required for the fusion competence of endoplasmic reticulum-derived vesicles. *The Journal of biological chemistry* **278**, 19878–19884.

22 Calero M, Winand NJ & Collins RN (2002) Identification of the novel proteins Yip4p and Yip5p as Rab GTPase interacting factors. *Febs Lett* **515**, 89–98.

23 Calero M & Collins RN (2002) Saccharomyces cerevisiae Pra1p/Yip3p interacts with Yip1p and Rab proteins. *Biochemical and Biophysical Research Communications* **290**, 676–681.

24 Soonthornsit J, Sakai N, Sasaki Y, Watanabe R, Osako S & Nakamura N (2017) YIPF1, YIPF2, and YIPF6 are medial-/trans-Golgi and trans-Golgi network-localized Yip domain family proteins, which play a role in the Golgi reassembly and glycan synthesis. *Experimental Cell Research* **353**, 100–108.

25 Tanimoto K, Suzuki K, Jokitalo E, Sakai N, Sakaguchi T, Tamura D, Fujii G, Aoki K, Takada S, Ishida R, Tanabe M, Itoh H, Yoneda Y, Sohda M, Misumi Y & Nakamura N (2011) Characterization of YIPF3 and YIPF4, cis-Golgi Localizing Yip domain family proteins. *Cell Struct Funct* **36**, 171–185.

26 Yoshida Y, Suzuki K, Yamamoto A, Sakai N, Bando M, Tanimoto K, Yamaguchi Y, Sakaguchi T, Akhter H, Fujii G, Yoshimura S, Ogata S, Sohda M, Misumi Y & Nakamura N (2008) YIPF5 and YIF1A recycle between the ER and the Golgi apparatus and are involved in the maintenance of the Golgi structure. *Experimental Cell Research* **314**, 3427–3443.

27 Sharp PM & Li W-H (1987) The codon adaptation index-a measure of directional synonymous codon usage bias, and its potential applications. *Nucleic Acids Res* **15**, 1281–1295.

28 Gingold H & Pilpel Y (2011) Determinants of translation efficiency and accuracy. *Mol Syst Biol* **7**, 481.

29 Hong D & Jeong S (2023) 3'UTR Diversity: Expanding Repertoire of RNA Alterations in Human mRNAs. *Mol Cells* **46**, 48–56.

30 Mayya VK & Duchaine TF (2019) Ciphers and Executioners: How 3'-Untranslated Regions Determine the Fate of Messenger RNAs. *Frontiers in genetics* **10**, 6.

31 Mayr C (2018) What Are 3' UTRs Doing? *Cold Spring Harbor Perspectives in Biology*, a034728.

32 Nakamura Y, Gojobori T & Ikemura T (2000) Codon usage tabulated from international DNA sequence databases: status for the year 2000. *Nucleic Acids Res* **28**, 292–292.

33 Hanson G & Coller J (2017) Codon optimality, bias and usage in translation and mRNA decay. *Nature Review Molecular Cell Biology* **19**, 20–30.

34 Wu Q & Bazzini AA (2023) Translation and mRNA Stability Control. *Annu Rev Biochem* **92**.

35 Shakoori A, Fujii G, Yoshimura S, Kitamura M, Nakayama K, Ito T, Ohno H & Nakamura N (2003) Identification of a five-pass transmembrane protein family localizing in the Golgi apparatus and the ER. *Biochem Biophys Res Commun* **312**, 850–857.

36 Portz B & Shorter J (2018) 3' UTRs in the Eye of the TIGER. *Dev Cell* **47**, 544–546.

37 Sheets MD, Ogg SC & Wickens MP (1990) Point mutations in AAUAAA and the poly (A) addition site: effects on the accuracy and efficiency of cleavage and polyadenylation in vitro. *Nucleic Acids Res* **18**, 5799–5805.

38 Bae H & Coller J (2022) Codon optimality-mediated mRNA degradation: Linking translational elongation to mRNA stability. *Mol Cell* **82**, 1467–1476.

39 Forrest ME, Pinkard O, Martin S, Sweet TJ, Hanson G & Coller J (2020) Codon and amino acid content are associated with mRNA stability in mammalian cells. *Plos One* **15**, e0228730.

40 Narula A, Ellis J, Taliaferro JM & Rissland OS (2019) Coding regions affect mRNA stability in human cells. *Rna* **25**, 1751–1764.

41 Hia F, Yang SF, Shichino Y, Yoshinaga M, Murakawa Y, Vandenbon A, Fukao A, Fujiwara T, Landthaler M, Natsume T, Adachi S, Iwasaki S & Takeuchi O (2019) Codon bias confers stability to human mRNAs. *Embo Rep* **20**, e48220.

42 Mishima Y & Tomari Y (2016) Codon Usage and 3′ UTR Length Determine Maternal mRNA Stability in Zebrafish. *Mol Cell* **61**, 874–885.

43 Harigaya Y & Parker R (2016) Codon optimality and mRNA decay. *Cell Res* **26**, 1269–1270.

44 Bazzini AA, Viso F del, Moreno-Mateos MA, Johnstone TG, Vejnar CE, Qin Y, Yao J, Khokha MK & Giraldez AJ (2016) Codon identity regulates mRNA stability and translation efficiency during the maternal-to-zygotic transition. *Embo J* **35**, 2087–2103.

45 Li W, Deng X & Chen J (2022) RNA-binding proteins in regulating mRNA stability and translation: roles and mechanisms in cancer. *Semin Cancer Biol* **86**, 664–677.

46 Mayr C (2017) Regulation by 3′-Untranslated Regions. *Annu Rev Genet* **51**, 171–194.

47 Otsuka H, Fukao A, Funakami Y, Duncan KE & Fujiwara T (2019) Emerging Evidence of Translational Control by AU-Rich Element-Binding Proteins. *Frontiers Genetics* **10**, 332.

48 Meyer J, Payr M, Duss O & Hennig J (2024) Exploring the dynamics of messenger ribonucleoprotein-mediated translation repression. *Biochem Soc Trans* **52**, 2267–2279.

49 Krshnan L, Weijer ML van de & Carvalho P (2022) Endoplasmic Reticulum–Associated Protein Degradation. *Cold Spring Harb Perspect Biol* **14**, a041247.

50 Berkovits BD & Mayr C (2015) Alternative 3’ UTRs act as scaffolds to regulate membrane protein localization. *Nature* **522**, 363–367.

51 Ma W & Mayr C (2018) A Membraneless Organelle Associated with the Endoplasmic Reticulum Enables 3’UTR-Mediated Protein-Protein Interactions. *Cell* **175**, 1492-1506.e19.

52 Leppek K, Das R & Barna M (2018) Functional 5′ UTR mRNA structures in eukaryotic translation regulation and how to find them. *Nat Rev Mol Cell Biol* **19**, 158–174.

53 Hinnebusch AG, Ivanov IP & Sonenberg N (2016) Translational control by 5′-untranslated regions of eukaryotic mRNAs. *Science* **352**, 1413–1416.

54 Moss MJ, Chamness LM & Clark PL (2023) The Effects of Codon Usage on Protein Structure and Folding. *Annu Rev Biophys* **53**, 87–108.

55 Ma X, Liu S, Fan B, Jin D, Miao L, Liu L, Du S & Lin J (2025) Enhancing mRNA translation efficiency by introducing sequence optimized AU-rich elements in 3′ UTR via HuR anchorage. *Mol Ther Nucleic Acids* **36**, 102485.

56 Green MR & Sambrook J (2012) *Molecular Cloning: A Laboratory Manual, Fourth Edition (3-Volume Set)* Cold Spring Harbor Laboratory Press;

57 Schneider CA, Rasband WS & Eliceiri KW (2012) NIH Image to ImageJ: 25 years of image analysis. *Nature Methods* **9**, 671–675.

Table I mRNA information of YIPF family proteins

YIPF	Relative Expression *1	Northern Blotting (bp) *2	RefSeq cDNA (bp)	3'UTR (bp)	CAI	RefSeq
a1A	1	3,600	3,395	2,235	0.67	NM_001024947
a 1B	30	ND	1170	326	0.72	NM_182592
a2	30	2,300	2,084	1,175	0.65	XM_011533125
a3	1	7,500	6,010	5,283	0.69	NM_173834
b1A	6	1,300	1,097	57	0.82	NM_020470
b1B	70	5,300	2,690	1,794	0.79	NM_001039672
b2	300	3,000	1,507	335	0.80	NM_015388
b3A	600	2,300	1,821	546	0.73	NM_018982
b3B	600	2,400	2,111	1,001	0.84	NM_001321439

*1: Relative values for YIPFα1A.

*2: Shakoori, A. *et al. Biochem Biophys Res Commun* **312**, 850–857 (2003).

Table II　Codon optimization of YIPFα1A

No.	WT	AA	Opt	No.	WT	AA	Opt	No.	WT	AA	Opt	No.	WT	AA	Opt
2	TCA	S	AGC	108	CTA	L	CTG	156	AGT	S	AGC	194	CTT	L	CTG
7	TTA	L	CTG	110	GTA	V	GTG	161	CTA	L	CTG	203	TTG	L	CTG
9	ACG	T	ACC	111	TTA	L	CTG	166	TTA	L	CTG	207	GTA	V	GTG
15	AGT	S	AGC	113	CCG	P	CCC	167	TTA	L	CTG	220	AGT	S	AGC
22	TCA	S	AGC	114	TTA	L	CTG	169	TTA	L	CTG	231	TTA	L	CTG
31	AGT	S	AGC	116	GTA	V	GTG	171	AGT	S	AGC	238	CTT	L	CTG
45	TCG	S	AGC	127	TTG	L	CTG	176	TCA	S	AGC	239	TTA	L	CTG
77	TCA	S	AGC	135	CTT	L	CTG	182	AGT	S	AGC	240	GTA	V	GTG
92	TTA	L	CTG	141	TTG	L	CTG	184	CCT	L	CTG	246	TTG	L	CTG
93	TTA	L	CTG	142	CTA	L	CTG	188	CTT	L	CTG	247	TTA	L	CTG
96	TTA	L	CTG	152	GTA	V	GTG	193	CTA	L	CTG				

* WT: CAI = 0.67, Opt: CAI = 0.82

Table III Mutation of predicted poly A sites

Mutant name	Base No.*1	WT	Mutant
Δ3	1010-1016	AAUAAA	AAUAAG
Δ4	1104-1110	AUUAAA	AUUAAG
Δ5	1260-1266	AUUAAA	AUUAAG
Δ6	1296-1302	AUUAAA	AUUAAG

*1: Counted from the 5' end of the 3'UTR

Table IV Statistical Significance*

M	1-1118	1116-2230	1-746	374-1118	1-373	374-746	747-1118	1-200	GAPDH
1-2230	NS	P<0.05	NS	P<0.01	NS	P<0.01	P<0.01	P<0.01	P<0.05
1-1118	-	NS	NS	P<0.05	NS	NS	P<0.01	P<0.01	NS
1116-2230	-	-	NS	NS	P<0.05	NS	P<0.05	P<0.01	NS
1-746	-	-	-	P<0.01	NS	P<0.05	P<0.01	P<0.01	NS
374-1118	-	-	-	-	P<0.01	NS	NS	P<0.01	NS
1-373	-	-	-	-	-	P<0.01	P<0.01	P<0.01	NS
374-746	-	-	-	-	-	-	NS	P<0.01	NS
747-1118	-	-	-	-	-	-	-	P<0.01	P<0.05
1-200	-	-	-	-	-	-	-	-	P<0.01

S	1-1118	1116-2230	1-746	374-1118	1-373	374-746	747-1118	1-200	GAPDH
1-2230	NS	NS	NS	NS	NS	NS	NS	P<0.01	P<0.05
1-1118	-	P<0.01	NS	P<0.05	P<0.01	P<0.01	P<0.05	P<0.01	P<0.01
1116-2230	-	-	P<0.05	NS	NS	NS	NS	P<0.01	NS
1-746	-	-	-	NS	P<0.05	P<0.05	NS	P<0.01	P<0.05
374-1118	-	-	-	-	NS	NS	NS	P<0.01	NS
1-373	-	-	-	-	-	NS	NS	P<0.01	NS
374-746	-	-	-	-	-	-	NS	P<0.01	NS
747-1118	-	-	-	-	-	-	-	P<0.01	NS
1-200	-	-	-	-	-	-	-	-	P<0.01

D	1-1118	1116-2230	1-746	374-1118	1-373	374-746	747-1118	1-200	GAPDH
1-2230	NS	P<0.01	NS	P<0.01	P<0.05	P<0.01	P<0.01	NS	P<0.01
1-1118	-	P<0.01	NS	P<0.01	NS	P<0.01	P<0.01	NS	P<0.01
1116-2230	-	-	P<0.01	NS	P<0.05	NS	P<0.05	P<0.01	NS
1-746	-	-	-	P<0.01	NS	P<0.01	P<0.01	NS	P<0.01
374-1118	-	-	-	-	P<0.01	NS	NS	P<0.01	NS
1-373	-	-	-	-	-	P<0.01	P<0.01	NS	P<0.05
374-746	-	-	-	-	-	-	NS	P<0.01	NS
747-1118	-	-	-	-	-	-	-	P<0.01	NS
1-200	-	-	-	-	-	-	-	-	P<0.01

*Statistical significance was determined using one-way ANOVA followed by Fisher's LSD test.

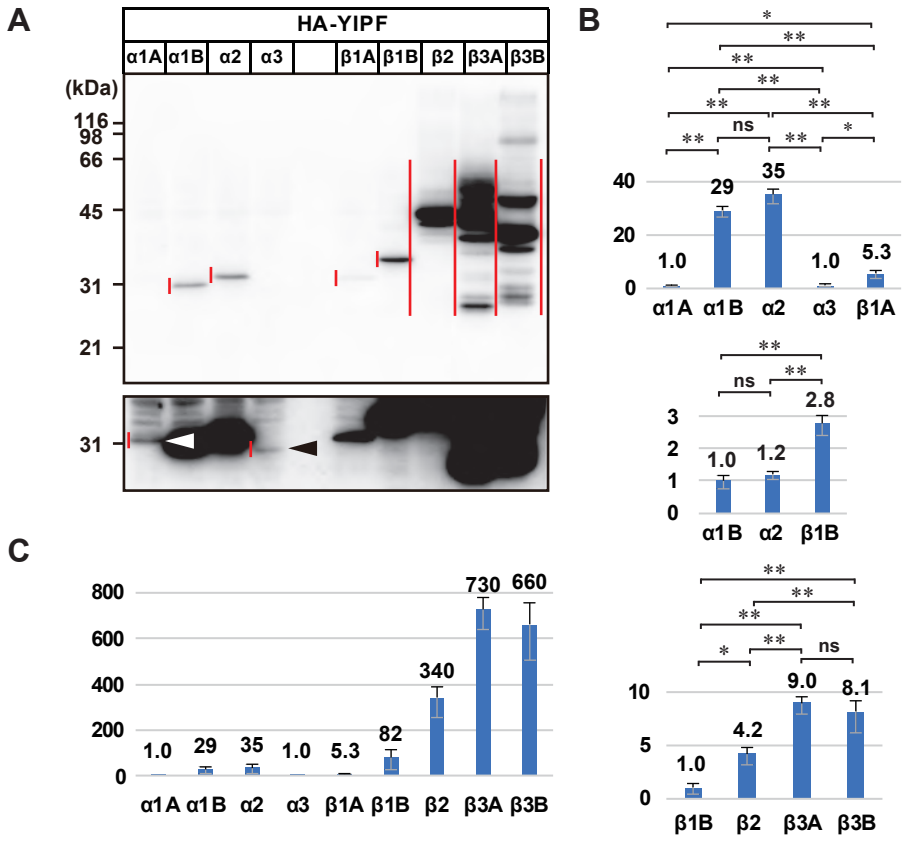
A
HA-YIPF
α1A α1B α2 α3 β1A β1B β2 β3A β3B
(kDa)
116
98
66
45
31
21
31
B
1.0 29 35 1.0 5.3
α1A α1B α2 α3 β1A
1.0 1.2 2.8
α1B α2 β1B
1.0 4.2 9.0 8.1
β1B β2 β3A β3B
C
1.0 29 35 1.0 5.3 82 340 730 660
α1A α1B α2 α3 β1A β1B β2 β3A β3B

Fig. 1

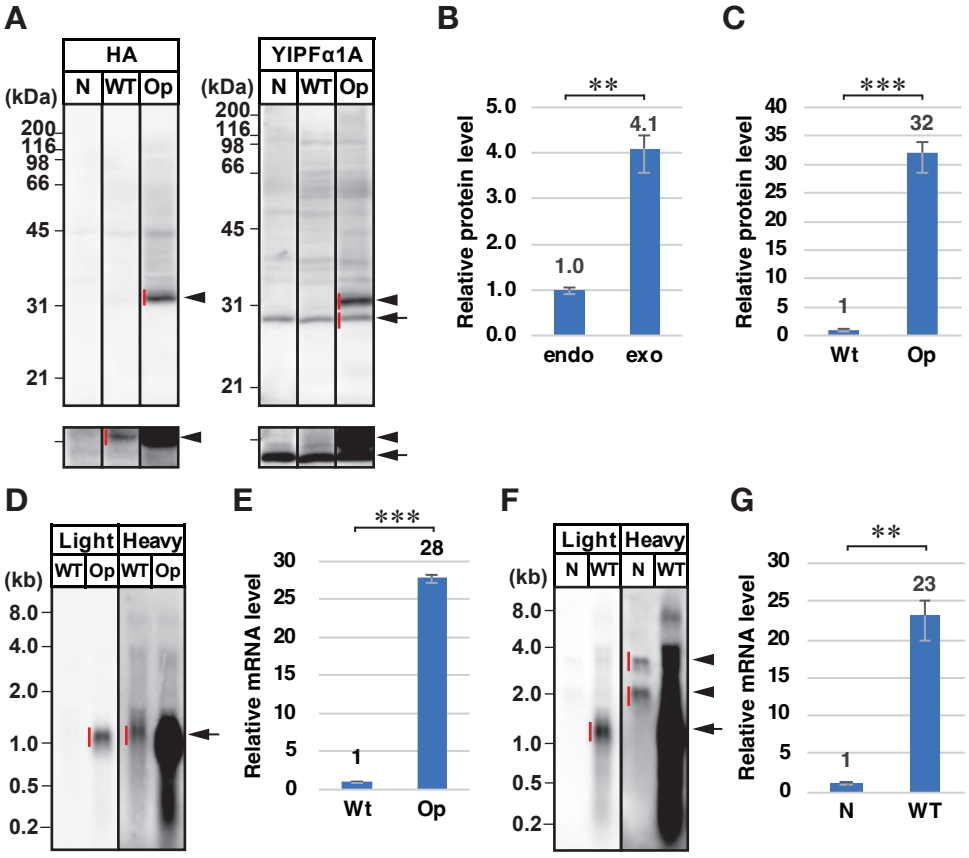
A
HA
N
WT
Op
(kDa)
200
116
98
66
45
31
21
YIPFα1A
B
Relative protein level
**
4.1
1.0
endo
exo
C
***
32
1
Wt
Op
D
Light
Heavy
(kb)
8.0
4.0
2.0
1.0
0.5
0.2
E
Relative mRNA level
28
F
G
23

Fig. 2

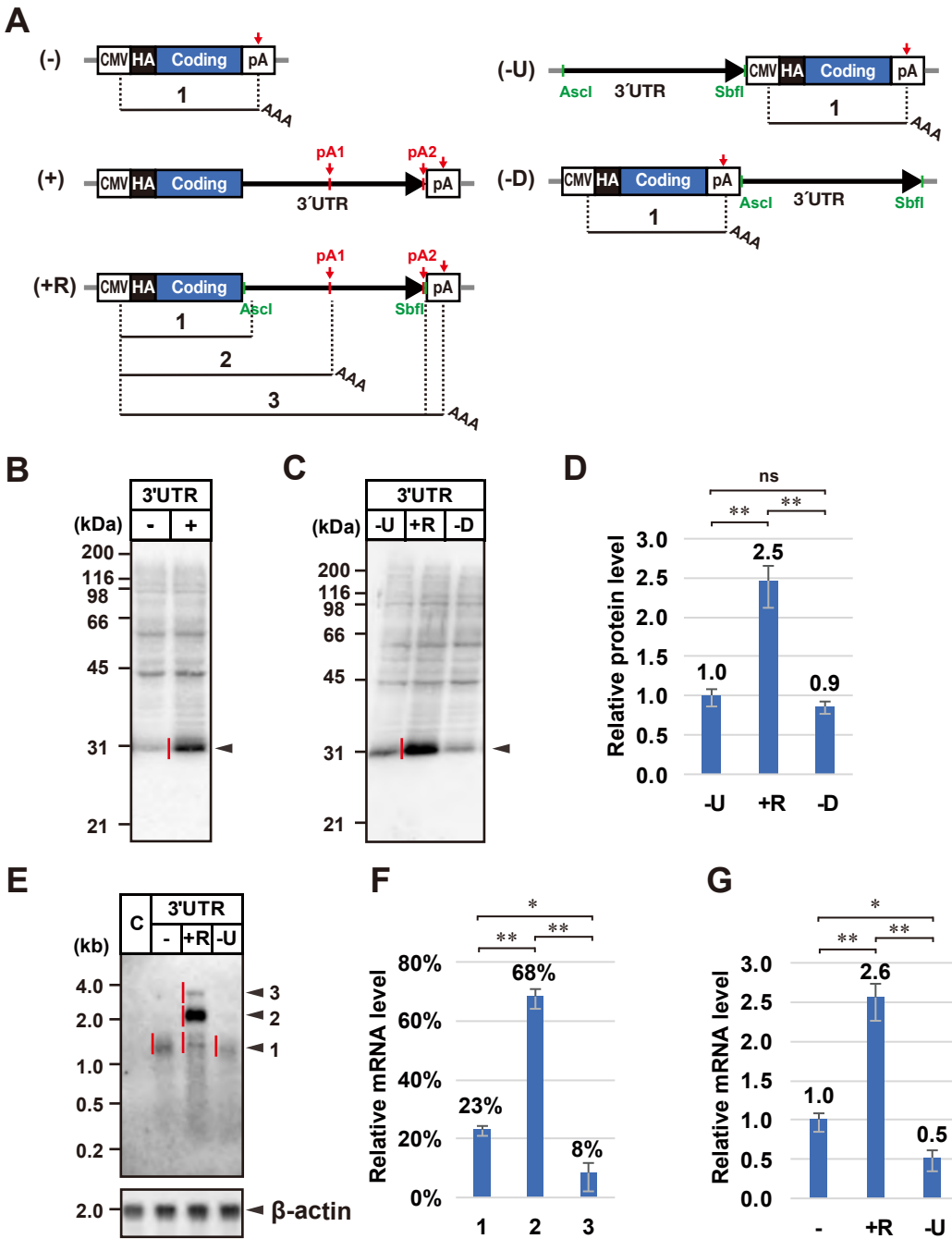
A
(-)
CMV
HA
Coding
pA
1
AAA
(+)
pA1
pA2
3´UTR
(+R)
AscI
SbfI
2
3
(-U)
(-D)
B
3'UTR
(kDa)
-
+
200
116
98
66
45
31
21
C
-U
+R
-D
D
Relative protein level
ns
**
2.5
1.0
0.9
E
C
(kb)
4.0
2.0
1.0
0.5
0.2
β-actin
F
Relative mRNA level
*
68%
23%
8%
G
2.6
0.5

Fig. 3

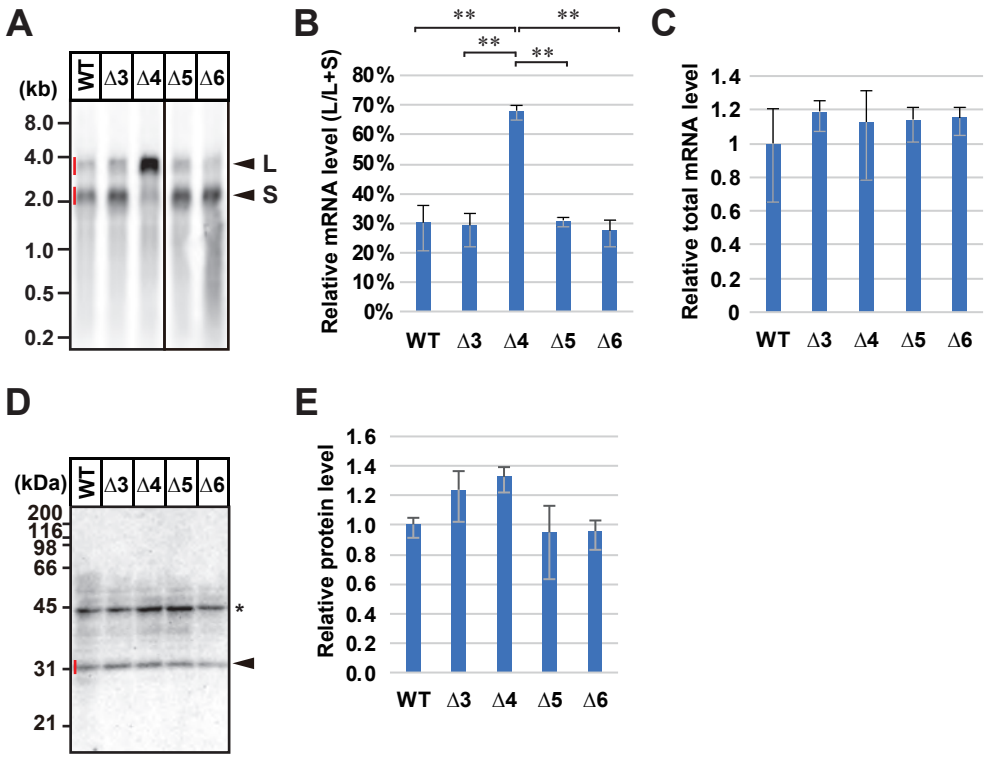
A
(kb)
WT
Δ3
Δ4
Δ5
Δ6
8.0
4.0
2.0
1.0
0.5
0.2
L
S
B
Relative mRNA level (L/L+S)
80%
70%
60%
50%
40%
30%
20%
10%
0%
**
**
**
**
WT
Δ3
Δ4
Δ5
Δ6
C
Relative total mRNA level
1.4
1.2
1
0.8
0.6
0.4
0.2
0
WT
Δ3
Δ4
Δ5
Δ6
D
(kDa)
WT
Δ3
Δ4
Δ5
Δ6
200
116
98
66
45
31
21
*
E
Relative protein level
1.6
1.4
1.2
1.0
0.8
0.6
0.4
0.2
0.0
WT
Δ3
Δ4
Δ5
Δ6

Fig. 4

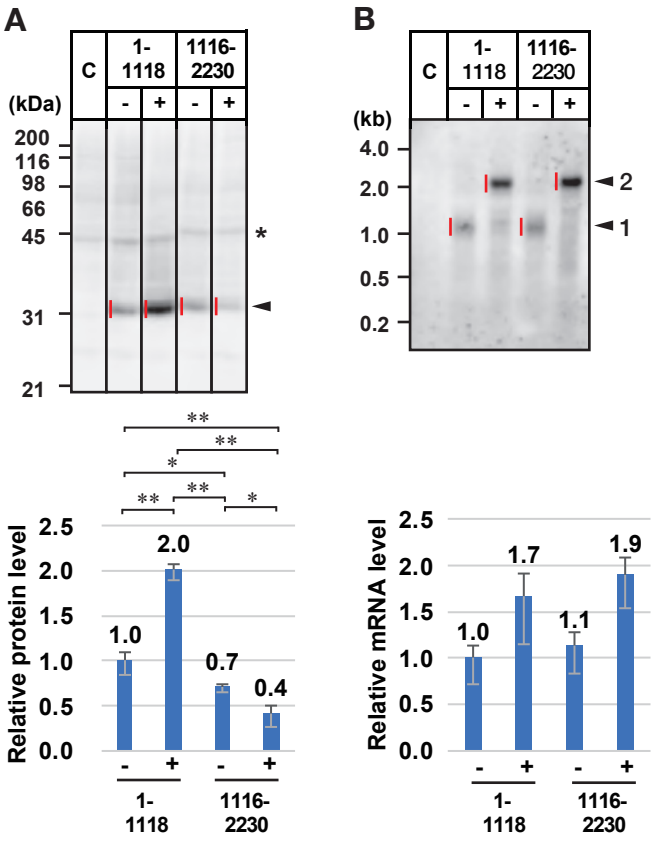
A
C
1-1118
1116-2230
(kDa)
200
116
98
66
45
31
21
*
Relative protein level
2.5
2.0
1.5
1.0
0.5
0.0
1.0
2.0
0.7
0.4
**
**
*
**
**
*
1-1118
1116-2230
B
(kb)
4.0
2.0
1.0
0.5
0.2
2
1
Relative mRNA level
1.0
1.7
1.1
1.9

Fig. 5

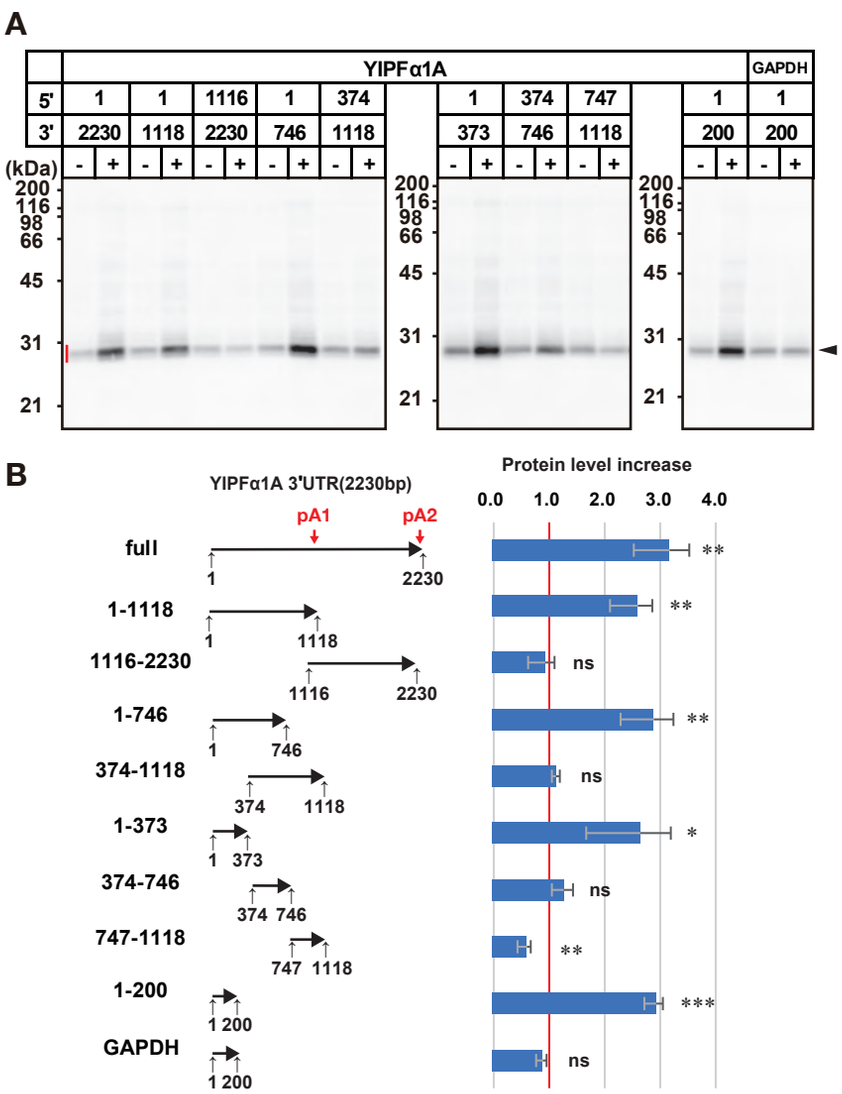
A
YIPFα1A
GAPDH
5'
3'
(kDa)
200
116
98
66
45
31
21
B
YIPFα1A 3'UTR(2230bp)
pA1
pA2
full
1-1118
1116-2230
1-746
374-1118
1-373
374-746
747-1118
1-200
GAPDH
Protein level increase
0.0
1.0
2.0
3.0
4.0
**
ns
*
***

Fig. 6

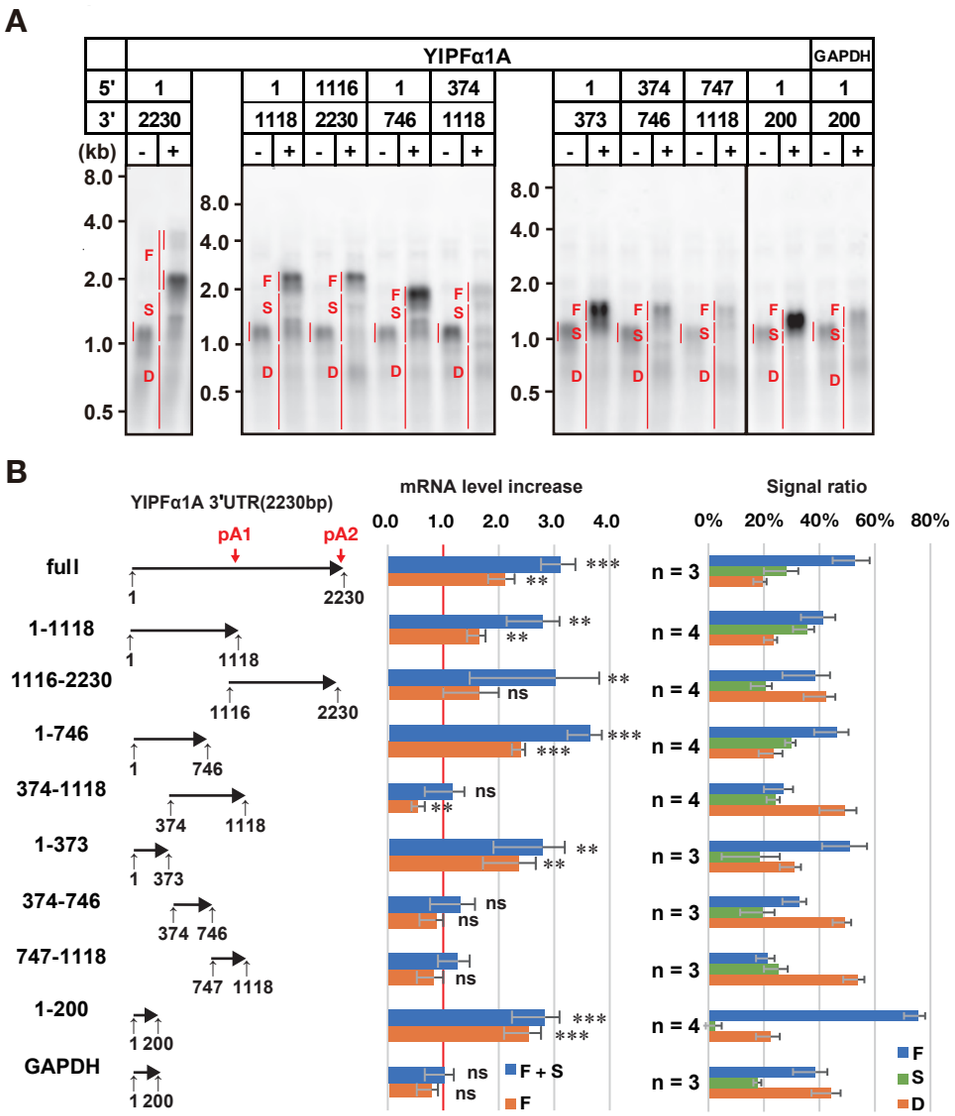
A
YIPFα1A
GAPDH
5'
3'
(kb)
1
2230
1116
1118
374
746
373
747
200
F
S
D
8.0
4.0
2.0
1.0
0.5
B
YIPFα1A 3'UTR(2230bp)
pA1
pA2
full
1-1118
1116-2230
1-746
374-1118
1-373
374-746
747-1118
1-200
GAPDH
mRNA level increase
Signal ratio
0.0
1.0
2.0
3.0
4.0
0%
20%
40%
60%
80%
n = 3
n = 4
ns
F + S
F
S
D

Fig. 7

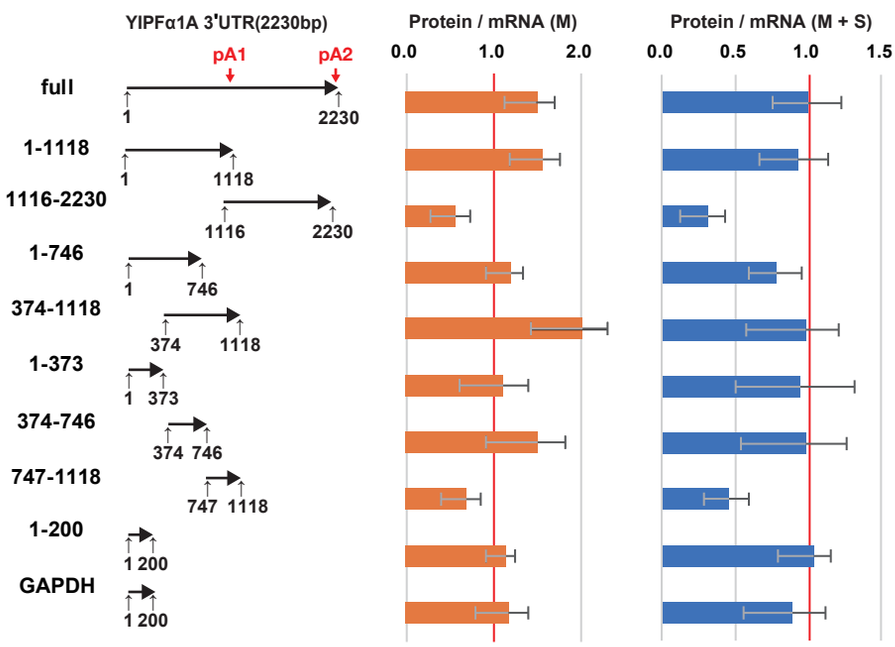
YIPFα1A 3'UTR(2230bp)
pA1
pA2
full
1
2230
1-1118
1
1118
1116-2230
1116
2230
1-746
1
746
374-1118
374
1118
1-373
1
373
374-746
374
746
747-1118
747
1118
1-200
1
200
GAPDH
1
200
Protein / mRNA (M)
0.0
1.0
2.0
Protein / mRNA (M + S)
0.0
0.5
1.0
1.5

Fig. 8